Neuro-regenerative behavior of adipose-derived stem cells in aligned collagen I hydrogels

Mackenzie Lewis [a], Gabriel David [a], Danielle Jacobs [a], Patrick Kuczwara [a,b], Alan E. Woessner [a], Jin-Woo Kim [b,c], Kyle P. Quinn [a], Younghye Song [a,*]

[a] Department of Biomedical Engineering; University of Arkansas, Fayetteville, AR, USA
[b] Department of Biological & Agricultural Engineering; University of Arkansas, Fayetteville, AR, USA
[c] Materials Science & Engineering Program; University of Arkansas, Fayetteville, AR, USA

ARTICLE INFO

ABSTRACT

Peripheral nerve injuries persist as a major clinical issue facing the US population and can be caused by stretch, laceration, or crush injuries. Small nerve gaps are simple to treat, and the nerve stumps can be reattached with sutures. In longer nerve gaps, traditional treatment options consist of autografts, hollow nerve guidance conduits, and, more recently, manufactured fibrous scaffolds. These manufactured scaffolds often incorporate stem cells, growth factors, and/or extracellular matrix (ECM) proteins to better mimic the native environment but can have issues with homogenous cell distribution or uniformly oriented neurite outgrowth in scaffolds without fibrous alignment. Here, we utilize a custom device to fabricate collagen I hydrogels with aligned fibers and encapsulated adipose-derived mesenchymal stem cells (ASCs) for potential use as a peripheral nerve repair graft. Initial results of our scaffold system revealed significantly less cell viability in higher collagen gel concentrations; 3 mg/mL gels showed 84.8 $\pm$ 7.3% viable cells, compared to 6 mg/mL gels viability of 76.7 $\pm$ 9.5%. Mechanical testing of the 3 mg/mL gels showed a Young's modulus of 6.5 $\pm$ 0.8 kPa nearly matching 7.45 kPa known to support Schwann cell migration. Further analysis of scaffolds coupled with stretching *in vitro* revealed heightened angiogenic and factor secretion, ECM deposition, fiber alignment, and dorsal root ganglia (DRG) neurite outgrowth along the axis of fiber alignment. Our platform serves as an *in vitro* testbed to assess neuro-regenerative potential of ASCs in aligned collagen fiber scaffolds and may provide guidance on next-generation nerve repair scaffold design.

1. Introduction

Peripheral nerve injury (PNI) remains a significant clinical challenge, with an average incidence of between 43 and 52 per one million people affected annually in the US alone [1,2]. While surgical coaptation of the severed ends of the nerves is possible in short- or no-gap injuries, long-gap injuries (20 mm or greater) require implantation of nerve repair grafts, including autografts, to avoid exerting excess tension on the remaining nerves and causing further damage. Nerve repair grafts are preferred over autografts to avoid additional surgery and corresponding sites of morbidity.

Current nerve repair implant strategies in the clinic are hollow nerve guidance conduits (NGCs) and decellularized nerve grafts [3]. While these strategies have been used to treat patients with nerve injuries, they do not provide universal solutions to nerve repair [4]. Hollow NGCs are

effective for short nerve gaps (less than 5 mm) [5]. On the other hand, decellularized nerve grafts such as Avance® nerve repair grafts have shown clinical success in longer gap repairs (up to 70 mm) because of the preservation of intraluminal basal lamina architecture. Nevertheless, decellularized nerve grafts possess a few limitations, including but not limited to 1) inability to tailor graft dimensions to individual patients, and 2) a need for migration of Schwann cells to facilitate axonal regeneration and axon myelination.

Aligned ECM fibers, particularly collagen, have been shown to enhance nerve repair potentials [6–9]. This has been demonstrated in not only engineered nerve repair grafts with aligned features, but also tissues such as tendons and muscles that contain aligned collagen fibers [10–12]. As such, there exist many different approaches to create aligned structures, including but not limited to uniaxial strain [13–16]; extracting longitudinal collagen fibers from inherently anisotropic

---

tissues [17,18]; extruding precursor solutions to induce alignment of polymer fibers [19–21]; and creating aligned patterns via alignment of dissolvable magnetic beads [10,11]. Among these different approaches, applying uniaxial strain to collagen pregel solutions offers the most simplistic approach to align both collagen fibers and encapsulated cells throughout an entire three-dimensional (3D) hydrogel.

Research into recellularization of acellular nerve grafts has been conducted using Schwann cells or mesenchymal stem cells (MSCs) from bone marrow (bMSCs) or adipose (ASCs), either undifferentiated or as Schwann-like cells, with abluminal coverage or endoneurial delivery using microinjectors [22–28]. While a direct injection of Schwann cells is beneficial, clinical translation of Schwann cell transplantation remains challenging because of the inherently low yield of autologous Schwann cells. While previous studies collectively show therapeutic benefits of MSC delivery in nerve-mimetic grafts, there still exists a need to develop grafts that allow an even distribution of MSCs across the graft containing basal lamina-like topographical features. Microinjections of MSCs at four or more sites along the length of the grafts have been widely used, yet this approach relies on migration of injected cells for homogeneous distribution across the entire length of the nerves. Further, while ASCs share many similarities with bMSCs, one key advantage of ASCs over bMSCs is their abundance and ease of isolation from stromal vascular fraction of adipose tissue [29], whereas harvesting bMSCs is a painful process yielding low cell counts [28,30].

Previous research suggests alignment of fibers could specifically enhance neuro-regenerative properties. For instance, aligned fibers doped with collagen [31–33] or growth factors [34,35] have been shown to promote neurite outgrowth. Further, Schwann cells and neurons embedded in hydrogels with aligned fibers exhibited increased neuro-regenerative potential [8,16,36]. Aligned fibers have also been shown to guide other tissue-reparative cells such as endothelial cells and macrophages to promote nerve repair activities of Schwann cells [37, 38]. Aligned fibers also accelerate neurogenic differentiation of stem cells including MSCs [19,39,40]. These studies collectively demonstrate neuro-regenerative benefits of aligned fibers. However, these studies were conducted for a relatively short period of time (mostly up to 3 days of culture *in vitro*) and neurite outgrowth assessments were done either in the absence of embedded cells or systemically *in vivo*. There still exists a knowledge gap on not only a broad range of neuro-regenerative behavior (e.g., viability, alignment, secretome, ECM composition, and resulting mechanical properties of the scaffolds) of ASCs in aligned collagen fiber hydrogels, but how these ASC-remodeled collagen gels influence neurite outgrowth.

Here, we explore neuro-regenerative behavior of ASCs in 3D hydrogels containing uniaxially aligned collagen fibers. To analyze the neuro-regenerative behavior of ASC-encapsulated hydrogels coupled with uniaxial strain, advanced culture systems were developed. To create aligned collagen fiber scaffolds, human ASCs were seeded into collagen I pregel solution, which was cast into a uniaxially stretched silicone mold. Thermally gelled 3D hydrogel scaffolds were cultured for 7 days before analysis was performed. We show directional alignment of ASCs with collagen fibers in stretched gels, and concomitant increase in neuro-regenerative ECM and cytokine deposition. Dorsal root ganglia (DRGs) were seeded onto gels after the 7-day culture period with ASCs to analyze neurite outgrowth. Overall, our study provides insight into neuro-regenerative behavior of ASCs in 3D aligned collagen I fiber scaffolds and further investigation may lead to the development of nerve repair scaffolds that contain nerve-mimetic intraluminal architecture and living depots of trophic factors.

2. Materials and methods

2.1. Collagen I pregel formation

Collagen I was isolated from frozen rat tails (VWR RLRBT297) based on a previously established method [41]. Skin was first removed from the tail, and each vertebra was pulled to isolate the tendons. The isolated tendons were digested in 0.1% acetic acid (Millipore Sigma 1000631000) at 75 mL/g for 3 days at 4 °C. The collagen digest was centrifuged in 40 mL volumes for 90 min at 8800 rpm and 4 °C. The supernatant was frozen for at least 24 h before being lyophilized (Labconco FreeZone 4.5) for 4 days. The resulting collagen I was digested in 0.1% acetic acid at a concentration of 10 mg/mL to create the pregel solution.

When used in hydrogel fabrication, 10% (v/v) 10x M199 (Sigma Aldrich M0650) were added to an aliquot of the pregel, followed by neutralization with 1M NaOH (Sigma Aldrich 415413). Phosphate buffered saline (PBS, VWR 97062) or cell suspension was then added to dilute to the working concentration for each sample. These pregels were then incubated at 37 °C to induce thermal gelation within their molds.

2.2. hASC culture

Human adipose-derived stem cells (hASCs, Lonza PT-5006) were cultured in ADSC Growth Medium Bulletkit (Lonza PT-3273 & PT-4503) containing 10% fetal bovine serum (FBS), 1% L-Glutamine, and 0.1% Gentamicin Sulfate-Amphotericin (GA-1000). All cultures were maintained at 5% CO_2 and 37 °C with media changes every 2–3 days. Cell passage p4-p5 were used for all cultures.

2.3. Aligned gels with ASCs

A custom stretching device was designed in SolidWorks and created with acrylic and steel (Fig. 1a). PDMS sheets (SMI 0.010″ NRV G/G 40D 12″X12″) were cut to the size of the silicone molds (Sigma Aldrich GBL664515) and plasma sealed using air plasma cleaner (Harrick Plasma) for >5 min (Fig. 1f). The PDMS-backed molds were clamped on both sides and placed on to the stretching device. The molds were then chemically functionalized to anchor collagen gels using a previously established method [42]; briefly, each well was filled with a 1% (v/v) solution of poly (ethyleneimine) (PEI, Sigma-Aldrich 181978) in ddH$_2$O for 10 min, 0.1% (v/v) glutaraldehyde (Sigma-Aldrich G6257) in ddH$_2$0 for 30 min, then rinsed twice with ddH$_2$O. The cell and pregel solution were then added to fill each well. The device and molds were incubated for 45 min at 37 °C to induce collagen gelation. The molds were removed from the stretching device and clamps and placed in small petri dishes 60 mm in diameter with 8 mL of hASC media to incubate for 7 days at 37 °C and 5% CO_2 with media changes every 48 h. After plasma cleaning, all steps were performed aseptically in a cell culture hood.

2.4. Quantitative Polarized Light Imaging (QPLI)

Quantitative Polarized Light Imaging (QPLI) was performed on a previously established QPLI microscope [43]. Briefly, circularly polarized light is transmitted through a rotating linear polarizer driven by a stepper motor to generate linearly polarized light. The light is then focused with a condenser lens, transmitted through the sample, and collected with a 4x (0.13 NA) objective. Using a fixed circular analyzer and camera after the objective, 10 images (2056 × 2056 pixels, 1.4 μm/pixel) were collected in 18° increments of the rotating linear polarizer, and the oscillation in intensity at each pixel was used to calculate a pixelwise fiber orientation and phase retardation. For this study, acellular stretched (S) and nonstretched (NS) gels with four different collagen I concentrations were placed on a microscope slide, covered with a coverslip, and imaged on the system. Due to the size of the gels, multiple images were collected and stitched together to create a full field of view for each gel, resulting in complete maps of fiber orientation and phase retardation. Following stitching of the images, masks were then generated by outlining the gel in the stitched image, and then applying a phase retardation threshold of 1°. To quantify fiber organization, an overall directional variance value, which is a measure of fiber organization ranging between 0 (anisotropic) and 1 (isotropic),
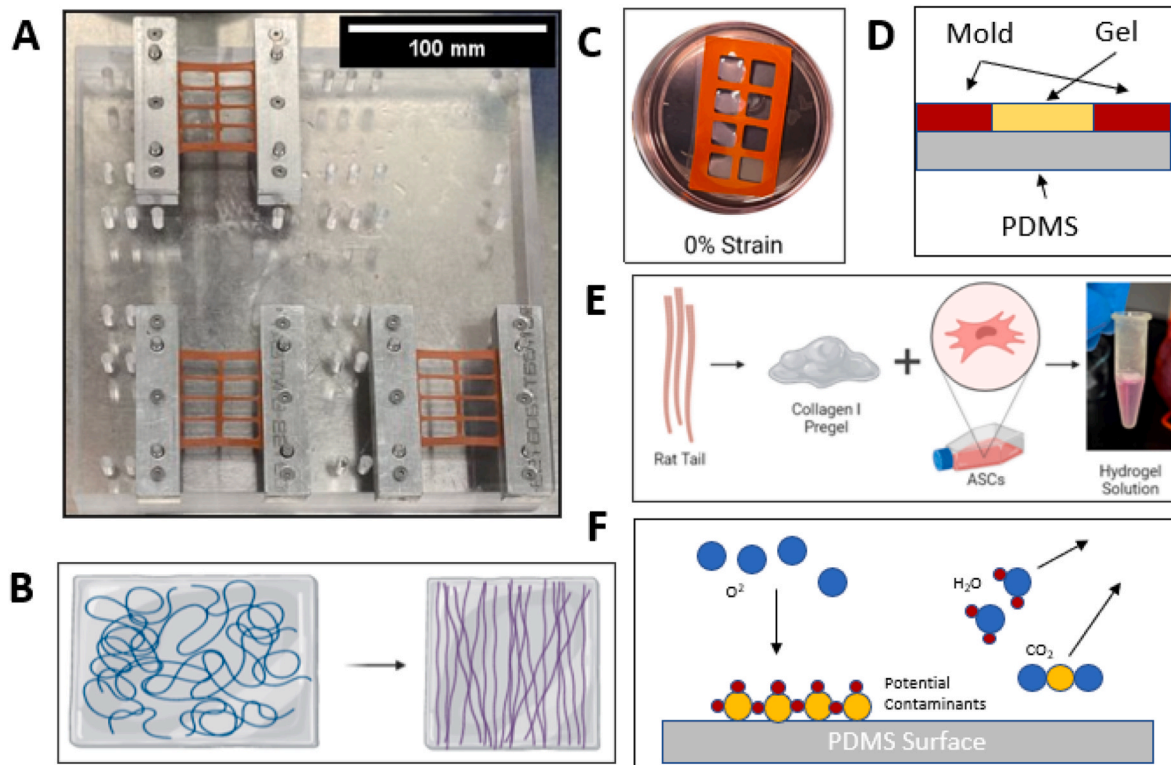
Fig. 1. A. Stretching device comprising acrylic base, steel clamps, and silicone molds. Scale bar = 100 mm **B.** Schematic showing the relaxation of the pre-stretched molds leading to aligned fibers. **C.** Silicone mold and gels in petri dish with media. **D.** Cross-section of silicone mold. **E.** Hydrogel creation process. **F.** Depiction of plasma cleaner sterilization and sealing methods. Figures B, C, and E created with BioRender.com.

was calculated from all fiber orientations within the generated mask.

2.5. Confocal reflectance microscopy

Acellular stretched and non-stretched hydrogels in 3 mg/mL and 6 mg/mL concentrations were created and fixed in 3.7% formaldehyde (Sigma-Aldrich 252549) in PBS at room temperature for 1 h. The gels were then rinsed and stored in PBS until imaging at 640 nm with an Olympus IX83 confocal microscope (20x objective magnification, $1.8\times$ digital zoom, NA 0.80) with a Z-step of 2 μm, starting from the 'top' surface and extending into the gel 250 slices or 500 μm. The resulting Z-stack was analyzed in ImageJ using the OrientationJ plugin. Evaluation within OrientationJ is based on the gradient structure tensor in an area within the region of interest [44]. The coherence of each sample was determined and used as a measure of alignment for the sample. Coherence values range from 0 to 1 and indicate orientation of image features, with 1 being anisotropic and 0 being entirely unaligned. For samples including immunofluorescence staining for cell and fiber co-alignment analysis, a Sobel-based orientation analysis was used for actin and collagen fiber alignment analysis, and the moment of inertia was used to determine the orientation of the nuclei. All values were binned at 10° from 0 to 180°, and summed bin values were normalized to the average value for that variable.

2.6. Immunofluorescence imaging

After 7 days of incubation, the gels were rinsed with PBS in their molds then fixed in 3.7% formaldehyde in PBS for 1 h. The gels were rinsed once with PBS for 5 min then transferred to a 24 well plate. Each well was rinsed with PBS 2 more times for 5 min each. The gels were then rinsed with 0.1% triton X-100 (Sigma-Aldrich 93443-100 ML) in PBS 2 times for 7 min. The gels were then incubated at room temperature with 1% bovine serum albumin (BSA, Sigma-Aldrich A7906-50G) in

PBS for 1 h. The gels were then allowed to sit overnight at 4 °C with the primary antibody solution diluted in 1% BSA. The gels were then rinsed 3 times with 0.1% Tween 20 (Sigma-Aldrich P9416-100 ML) in PBS for 5 min. Gels were then protected from light and incubated for 1 h at room temperature with a secondary antibody solution in 1% BSA. The gels were then rinsed twice for 5 min with 0.1% Tween 20 and once with PBS before being stored in fresh PBS.

Antibodies were purchased from Thermo Fisher unless otherwise stated, and their dilutions are listed as follows: DAPI (1:2500, D1306), Phalloidin 546 (1:500, A22283), Phalloidin 488 (1:500, A12379), anti-rabbit Laminin (1:200, PA1-16730), anti-mouse Fibronectin (1:200, MA5-11981), anti-mouse Yes-associated Protein (1:500, Santa Cruz Biotechnology, sc-101199), anti-mouse Neurofilament (1:500, Developmental Studies Hybridoma Bank, RT97), Alexa Fluor goat anti-mouse 488 (1:500, A11029), Alexa Fluor 488 goat anti-rabbit (1:500, A11008), Alexa Fluor goat anti-mouse 568 (1:500, A11031), Alexa Fluor goat anti-rabbit 568 (1:500, A11011), Alexa Fluor goat anti-mouse 647 (1:500, A21235), and Alexa Fluor goat anti-rabbit 647 (1:500, A21244). DAPI was used to show the presence of cells while also showing differences in cell density. Phalloidin, staining actin fibers, provides an insight into the alignment of ASCs in the stretched and non-stretched gels. Neurofilament stains DRG neurites for direction and length analysis. Laminin and fibronectin antibodies were used to show the ECM deposition and alignment of cell-laden gels. Fluorescence imaging was performed with an Olympus IX83 confocal microscope (20x objective magnification, NA 0.80) with a Z-step of 2 μm, starting from the 'top' surface and extending into the gel 250 slices or 500 μm.

2.7. Live/dead assay

To determine cell viability in the scaffolds, 50 μL of Live/Dead solution (Fisher Scientific R37601) was added to each gel in the mold for 15 min. The gels were then suspended in clear Dulbecco's Modified

Eagle Medium (DMEM, Fisher Scientific 12-800-017) until imaging. Each gel was removed from its mold and placed on a microscope slide for imaging with an Olympus IX83 confocal microscope (20x objective magnification, NA 0.80) with a Z-step of 5 μm, starting from the 'top' surface and extending into the gel 100 slices or 500 μm. The percentage of live and dead cells was calculated with a custom MATLAB code quantifying the area occupied by live and dead cells. Analysis was performed on the compressed Z-stack at max intensity.

2.8. Luminex

Serum-free ASC media were added to gels and collected after 24 h to analyze hASC secretome. The conditioned media were briefly spun to remove cell debris, followed by tenfold concentration using Amicon Ultra-4 Centrifugal Filter (3 kDa MWCO, Millipore Sigma UFC800396). Custom-designed 4-Plex Luminex kits (R&D Systems) were used to quantify beta-nerve growth factor (βNGF), neurotrophin-3 (NT-3), glial-derived neurotrophic factor (GDNF), and brain-derived neurotrophic factor (BDNF) as well as hepatocyte growth factor (HGF), basic fibroblast growth factor (FGF-2), angiopoietin-1 (Ang-1), and interleukin-8 (IL-8) levels in the conditioned media. Resulting values were normalized to double-stranded DNA (dsDNA) content. DNA concentration was determined using DNeasy Blood and Tissue Kit (Qiagen 69504) to isolate dsDNA and Quantifluor dsDNA System (Promega E2670) to quantify DNA content.

2.9. YAP staining analysis

Quantitative analysis of immunofluorescence images stained against YAP was performed by creating a Z-stack of slices 10–30 in ImageJ with constant minimum and maximum values for both YAP and DAPI intensity. These images were exported to MATLAB for analysis with a custom code determining the intensity of staining in the nuclear and cytoplasmic regions of the cells.

2.10. Mechanical testing

Acellular and cellular 1 million (M) cell/mL, 3 mg/mL hydrogels were used for rheologic testing after 7 days of incubation. A Discovery Hybrid Rheometer (DHR-2) equipped with 25 mm compression plate (TA Instruments, New Castle, DE) was used to test the viscoelastic properties of collagen gels. A plate gap of 1 mm was set before the gels were compressed a total distance of 995 μm at a rate of 31.5 μm/s. Data was collected in Trios software provided by TA Instruments and exported to Excel for analysis. The Young's Moduli were determined from the linear portion of the graphs.

2.11. DRG harvest and dissociation

All animal work was approved by the Institutional Animal Care and Use Committee (IACUC) of the University of Arkansas (protocol numbers 23019 and 20054). Male Sprague Dawley rats (3–4 weeks) weighing 35–49 g were purchased from Envigo and cared for by staff of the South Campus Animal Facility in accordance with the IACUC Standards and the Animal Welfare Act. Rats had access to 12-h light/dark cycles and standard food and water *ad libitum*. Rats were euthanized in ordinance with the American Veterinary Medical Association guidelines via carbon dioxide asphyxiation.

2.11.1. Harvest methods
Immediately following euthanasia, the rat was transferred to a sterile hood and placed on an absorbent mat for dissection and DRG harvest. The rat was then sprayed with 70% ethanol, and electric clippers were used to shave the dorsal side of the animal. The skin was removed from the dorsal muscle and fascia with surgical scissors. Bone cutters were then used to sever the spinal column in the cervical and lumbar regions

then to isolate the spinal column by cutting on either side of the of the spine from the cervical to lumbar dislocations. Following removal of the spinal column and trimming of any extra muscle, the spinal cord was removed via hydraulic extrusion with a 3 mL syringe and PBS. Surgical scissors were then used to cut through the dorsal and thoracic sides of the spinal column, allowing for the lateral halves to be separated. The DRGs were visualized and removed carefully with sterile forceps, cleaned and trimmed, and then collected in hibernate media (Thermo Fisher, A1247501) on ice until use.

2.11.2. Dissociation methods
Dissociation and coculture of the DRGs are adapted from a previously established method [45]. First, the DRGs were collected in a microtube with 0.1% trypsin (Thermo Fisher, 15400054) and 1 mg/mL collagenase (Millipore Sigma, 10103578001) in PBS and allowed to incubate at 37 °C for 50 min, agitating the microtube every 10 min. The microtube was then centrifuged at 300 g for 5 min. The supernatant was subsequently removed and replaced with a suspension of 0.1% trypsin in PBS and allowed to incubate at 37 °C for 10 min. After incubation, neurobasal media supplemented with 1% Pen/Strep (Thermo Fisher, 15-140-122) and 2% B27 (Thermo Fisher, A3582801) were added to the microtube at a 3:1 ratio (media: PBS), and the microtube was centrifuged again. The final supernatant was removed and replaced with fresh supplemented neurobasal media. The partially dissociated DRGs were resuspended in the solution and kept on ice until coculture.

2.12. Neurite outgrowth model and quantification

2.12.1. Coculture methods
Acellular and cellular scaffolds were incubated for 7 days in ADSC media before neuron coculture. Immediately prior to seeding, media were removed from the hydrogels. A second sterile silicone isolator was placed atop the original, raising the outer wall of the mold. A 50 mL suspension of neuron media containing one intact DRG was then added to each individual hydrogel and contained within the added isolator. The DRGs were moved to the center of the hydrogel if needed. The DRGs were allowed to incubate without additional media for 12 h at 37 °C to assist in anchoring of the DRG to the scaffold [45]. After 12 h, 6 mL of supplemented neuron media were then added to the hydrogels, ensuring no DRGs are displaced in the process, and incubated for another 36 h at 37 °C until fixation and staining. Immunofluorescence staining of the hydrogel cocultures was performed with *anti*-neurofilament antibodies for neurite visualization and phalloidin for ASCs.

2.12.2. Quantification
Overall orientation of DRG outgrowth was performed on a Z-stack of the entire Neurofilament channel in ImageJ with the Distribution tool in the OrientationJ plugin, which provides an orientation degree for each non-zero pixel. Histogram values were binned in 10-degree increments. Quantification of neurites was performed in FIJI using the Sholl analysis tool in the SNT plugin with a step size of 100 μm. The center of the DRG was used as the starting point, and neurites were quantified from 100 to 1400 μm.

2.13. Statistical analysis

Statistical analysis was performed in GraphPad Prism 9.5.1 using unpaired t-tests, one-, two-, and three-way ANOVAs with Tukey's post-hoc analysis. Statistical significance was determined at $p < 0.05$.

3. Results and discussion

3.1. Physical properties

3.1.1. Fiber alignment analysis
We assessed collagen fiber alignment using QPLI and confocal

reflectance. QPLI is a popular imaging method used to determine orientation of birefringent fibers within tissues and samples. To optimize our hydrogel composition for subsequent cell culture, QPLI was performed on stretched and non-stretched samples in collagen hydrogel concentrations of 1, 2, 3, and 6 mg/mL to examine the collagen fiber alignment (n = 4 per group). The 1 and 2 mg/mL hydrogel samples failed to hold their shape and alignment after being released from the stretching device, and thus had no significant change in directional variance resulting from stretching. Directional variance measured with QPLI revealed significant decrease in variance (increase in alignment) after stretching in the 3 and 6 mg/mL samples (Fig. 2a). Both 3 and 6 mg/mL samples maintained their shape and structure after being released from the stretching device.

To support our findings from QPLI, we performed confocal reflectance imaging on both stretched and non-stretched samples in 3 and 6 mg/mL concentrations to visualize individual collagen fiber organization and structure within the hydrogels. Imaging and analysis revealed significant increases in collagen fiber organization and alignment in both the 3 mg/mL and 6 mg/mL stretched samples compared to non-stretched controls (Fig. 2b). Reflectance imaging of the collagen fibers resulted in organization that can be visualized at a macro-scale but is composed of many disconnected pixels that make analysis with pixel-based tools challenging. Due to this disconnection, the objective values for coherence of all reflectance samples, while indicating increased alignment, were lower than those seen in full fiber (actin) analysis. Similar results indicating an increase in alignment were seen with Sobel and Fourier analyses performed in MATLAB.

Through QPLI and confocal reflectance imaging, we hereby demonstrate a significant increase in fiber alignment with the use of our stretching device. This result aligns with other studies achieving hydrogel fiber alignment through the usage of uniaxial stretch and compression [8,14]. Many of these studies utilize a one-piece, flexible PDMS mold that can be pre-stretched or pre-compressed, for the hydrogel to then be cast in and relaxed from. Unlike many of these studies, we have employed a two-part mold, comprising a silicone isolator and silicone sheet backer. This allows for easier removal of the hydrogels and their usage as a scaffold, as opposed to only an *in vitro* testbed.

3.2. ASC response

3.2.1. Cell alignment

After 7 days of incubation, 3 and 6 mg/mL hydrogels were stained with phalloidin to assess cell alignment within the hydrogels (Fig. 3a). Image analysis revealed a significant increase in alignment in the stretched samples compared to the control in all cell densities and collagen concentrations tested (Fig. 3b–c). There was an increase in cell alignment in the 6 mg/mL 1 M samples compared to the same density in 3 mg/mL, but we did not see any significant difference in the 2 M samples (Fig. 3d).

To confirm that cell alignment was coherent with collagen fiber alignment, we performed confocal reflectance imaging along with immunofluorescence to visualize cells and fibers together (Supplementary Figure 1a). Upon qualitative visualization of these results, we
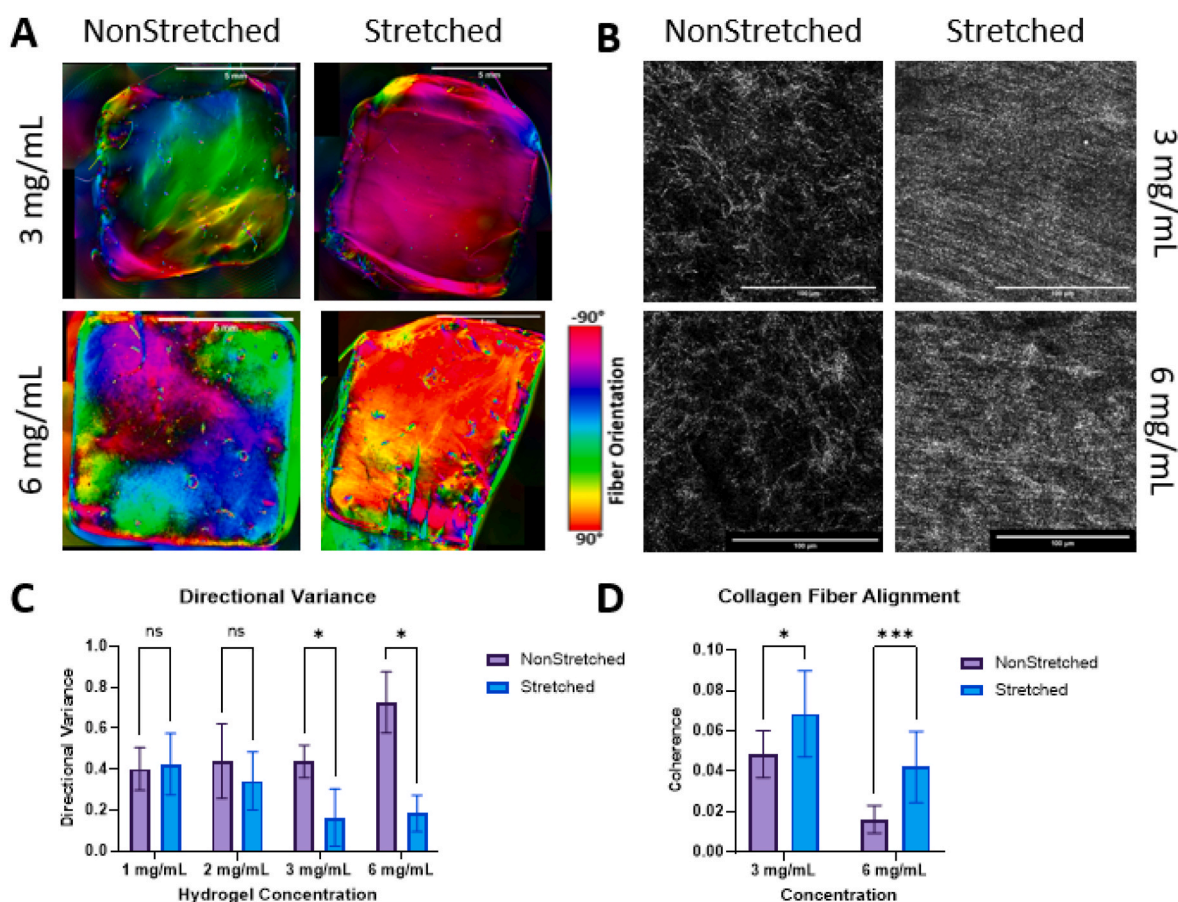

Fig. 2. A. QPLI microscope images depicting fiber orientation in scaffolds after 1 day of culture, red is vertical fibers and cyan is horizontal. Scale bar = 5 mm. **B.** Confocal reflectance images visualizing collagen I fibers in acellular hydrogels after 2 days of culture. Scale bar = 100 μm. **C.** Graph showing the directional variance of samples with and without stretching. Analysis performed with multiple t-tests, *p<0.05 for n = 4/group. **D.** Graph showing the coherence (uniformity) for each sample group. Analysis performed with multiple t-tests, *p<0.05, ****p<0.001 for n = 12/group. (For interpretation of the references to color in this figure legend, the reader is referred to the Web version of this article.)
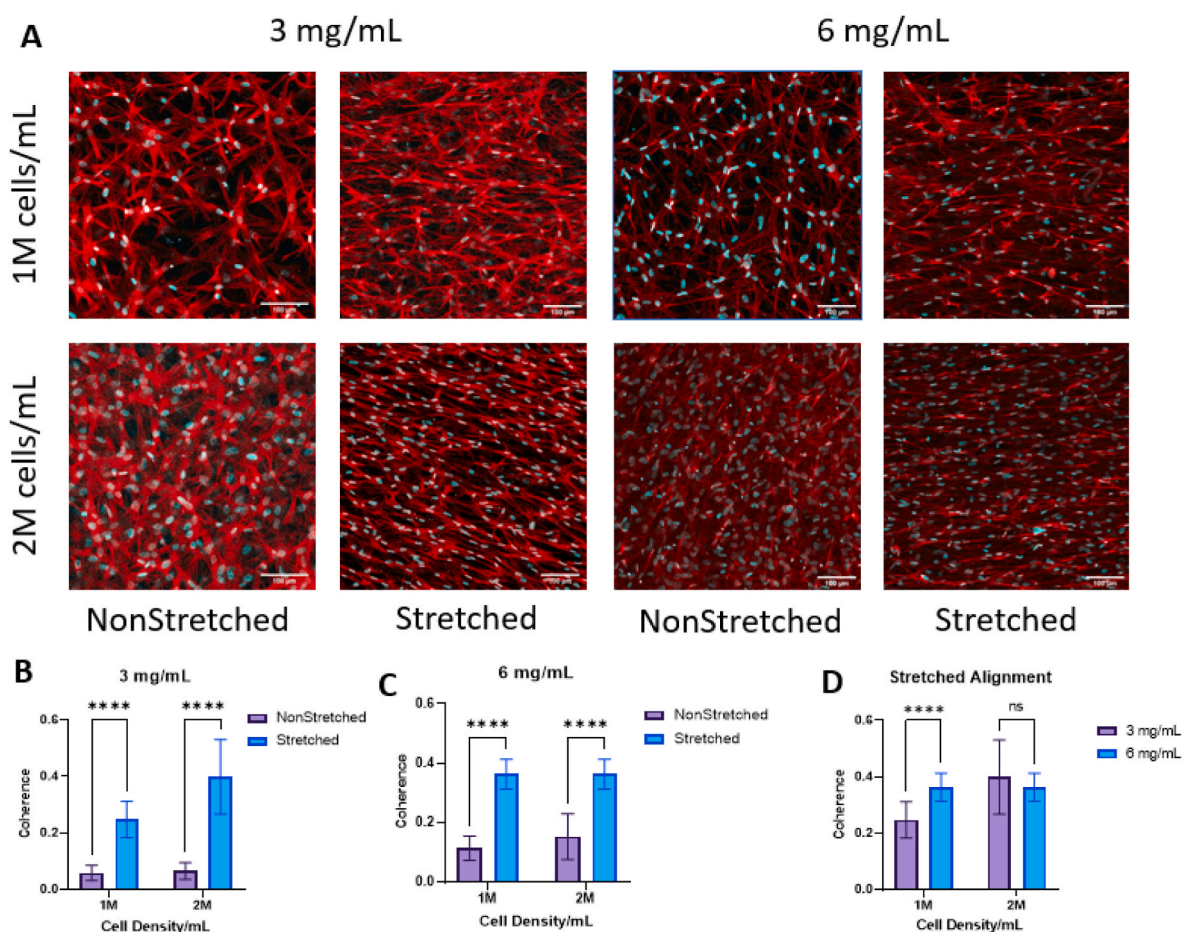
Fig. 3. A. Images of cells in the bulk of the hydrogel after 1 week of culture, stained with phalloidin (red) to visualize f-actin and the cell body and with DAPI (blue) to visualize cell nuclei. Scale bar = 100 μm **B, C.** Graph depicting the coherence (alignment) of actin fibers within (**B**) 3 mg/mL and (**C**) 6 mg/mL samples. **D.** Graph showing the coherence of actin fibers within stretched scaffolds for 3 and 6 mg/mL and 1 and 2 M/mL. Analysis performed with multiple t-tests. ****p<0.0001 for n = 12/group. (For interpretation of the references to color in this figure legend, the reader is referred to the Web version of this article.)

determined that cells were aligned uniformly along the direction of collagen fibers. Quantitative analysis in MATLAB shows co-localization of actin, collagen, and nuclei in the stretched 3 and 6 mg/mL samples that is not seen in either nonstretched group, indicated by the peak of both stretched group histograms around 90° (Supplementary Figure 1b). This result is also in agreement with previous studies who have found co-alignment of encapsulated cells with scaffold fibers [14,46]. Not only can fiber alignment affect cell behavior and alignment, but this organization can provide structural guidance for outgrowing nerves to follow.

3.2.2. Cell viability

After demonstration of collagen fiber alignment within the hydrogels, hASCs were added to the pregel before thermal gelation to allow for alignment of the embedded cells. To assess cell viability within the hydrogels, a live/dead assay was performed after 7 days of culture (Fig. 4a). The assay revealed a significantly higher cell viability in the 3 mg/mL hydrogels compared to the 6 mg/mL samples (Fig. 4c). Within each group, there was no difference in viability relating to cell density or stretched vs. control samples (Fig. 4d–e). This is in agreement with published literature, with studies investigating the effects of both cell density and substrate alignment seeing no influence on viability from either factor [46]. So, while fiber alignment may influence cell morphology and behavior, it does not positively or negatively influence cell survival. Therefore, since cell viability is significantly less in 6 mg/mL samples, 3 mg/mL gels were chosen for further analysis.

3.3. ECM deposition and cell secretome

3.3.1. Cell secretome

Conditioned media collected from 7-day hydrogel culture after 24 h were analyzed with custom 4-plex Luminex kits (neurotrophic - NT-3, βNGF, GDNF, and BDNF; angiogenic - HGF, FGF-2, Ang-1, and IL-8) for hASC secretome in 3 mg/mL hydrogels with 1 and 2 M/mL cell densities. NT-3 was excluded due to absence of expression in Luminex results. The 1 M/mL hydrogels showed significant increase in all analytes in the stretched samples compared to non-stretched for both neurotrophic and angiogenic factors (Fig. 5). The 2 M/mL samples showed an increase in all angiogenic analytes as well as BDNF and GDNF in the stretched samples compared to the control (Fig. 5).

Growth factors have been proven to be vital for translatable success with implantable peripheral nerve repair scaffolds [47]. Several studies have investigated the secretome response to cell culture in aligned substrates, and many saw increases in various immunomodulatory and angiogenic factors in bMSCs and ASCs [48,49]. Neurotrophic factors, such as those mentioned above, have been proven to increase neurite outgrowth and functional outcomes in peripheral nerve repair applications [50,51], but no studies have investigated the influence of fiber alignment on bMSC or ASC neurotrophic secretome. As previously mentioned, both fiber alignment and embedded cells may influence neuro-directed stem cell differentiation, which may be positively influencing cell secretome.

In peripheral nerve repair, BDNF, GDNF, and NGF are well documented in literature and act to encourage proliferation, survival, and
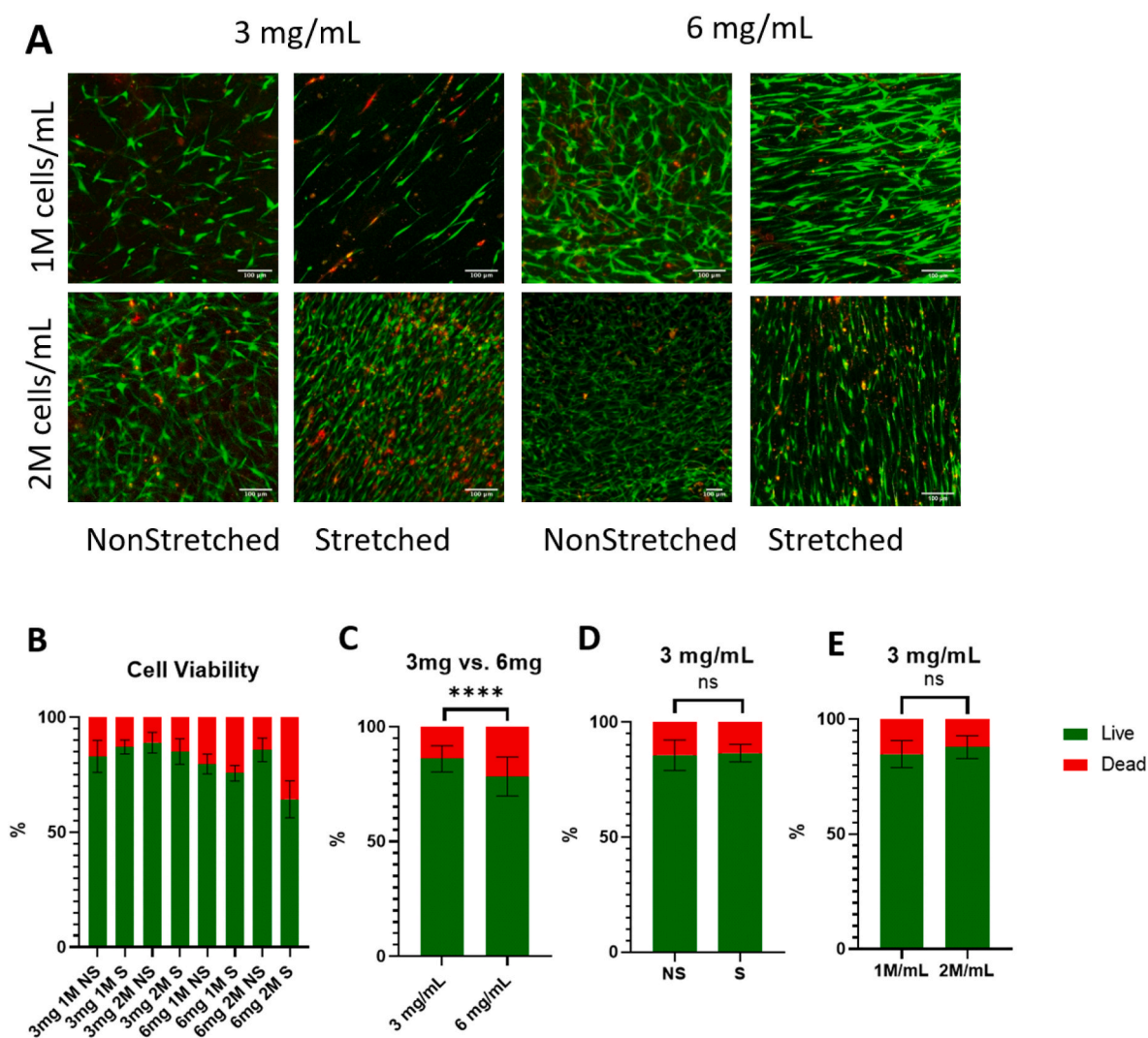
Fig. 4. A. Images showing live (green) and dead (red) cells within the scaffolds after 1 week of culture. Scale bar = 100 μm **B.** Graph showing the percentage of live and dead cells within the scaffolds. Analysis performed with a one-way ANOVA and post-hoc Tukey's test. **C.** Graph showing the percentage of live and dead cells in all 3 and 6 mg/mL samples. Analysis performed with *t*-test. ****$p < 0.0001$ for $n = 28$–34/group. **D, E.** Graph showing the percentage of live and dead cells in 3 mg/mL samples, comparing (**D**) non-stretched (NS) and stretched (S) samples, and (**E**) 1 and 2 M/mL samples. Analysis performed with *t*-test. ns = no significance. (For interpretation of the references to color in this figure legend, the reader is referred to the Web version of this article.)

expression of peripheral neurons [50,51]. In addition to the benefits provided by the neurotrophic factors, the secreted angiogenic factors benefit peripheral nerve repair. Basic fibroblast growth factor (FGF-2) has been well documented in wound repair and vascularization, but supplementation of FGF-2 also has been proven to increase functional and morphologic outcomes such as myelination and Schwann cell proliferation after peripheral nerve injury [52]. While IL-8 is associated with both anti- and pro-inflammatory mechanisms and occasionally linked to pain at the injury site, studies have shown that increased IL-8 helps to recruit immune cells vital in wound healing and acts as an angiogenic factor encouraging vascularization, and the presence of which may be indicative of ASC to Schwann cell differentiation [53–55]. In another study, inclusion of Ang-1 was able to establish vascularization early in peripheral nerve repair and is one of the two main factors in vascularization (VEGF being the other) [56]. HGF has been shown in additional studies to be vital in myelination thickness and axonal regrowth. It also promotes the proliferation and migration of Schwann cells and increases expression of endogenous GDNF [57,58].

Encapsulation of cells stands as an attractive alternative to direct growth factor inclusion in scaffolds or local injection. Previously, growth factors have been administered at the site of injury with some

success [47,50]. However, those factors are typically exhausted or not retained at the site of injury. A construct with encapsulated growth factors can ensure localization to the site of injury, but the growth factors will still be exhausted over time. In cellular scaffolds, the embedded cells will continue to produce growth factors as long as cell viability is maintained. Another advantage of encapsulating cells directly, compared to growth factor encapsulation, is that multiple physiologically relevant growth factors can be incorporated with more ease than in acellular scaffolds. Furthermore, stem cells like ASCs have the potential to differentiate into tissue-like cells supporting native tissue regeneration and natural secretome deposition during scaffold degradation.

Results indicate a significant increase of all analytes, both angiogenic and neurotrophic in the stretched 1 M/mL samples compared to only an increase in the angiogenic factors plus BDNF and GDNF in the stretched 2 M/mL gels. Because of less analyte upregulation in the 2 M/mL sample group, we selected the 1 M/mL sample group for further characterization and experiments.

3.3.2. ECM deposition

After 7 days of incubation, 3 mg/mL hydrogels in 1 and 2 M/mL cell densities were stained with antibodies against fibronectin and laminin
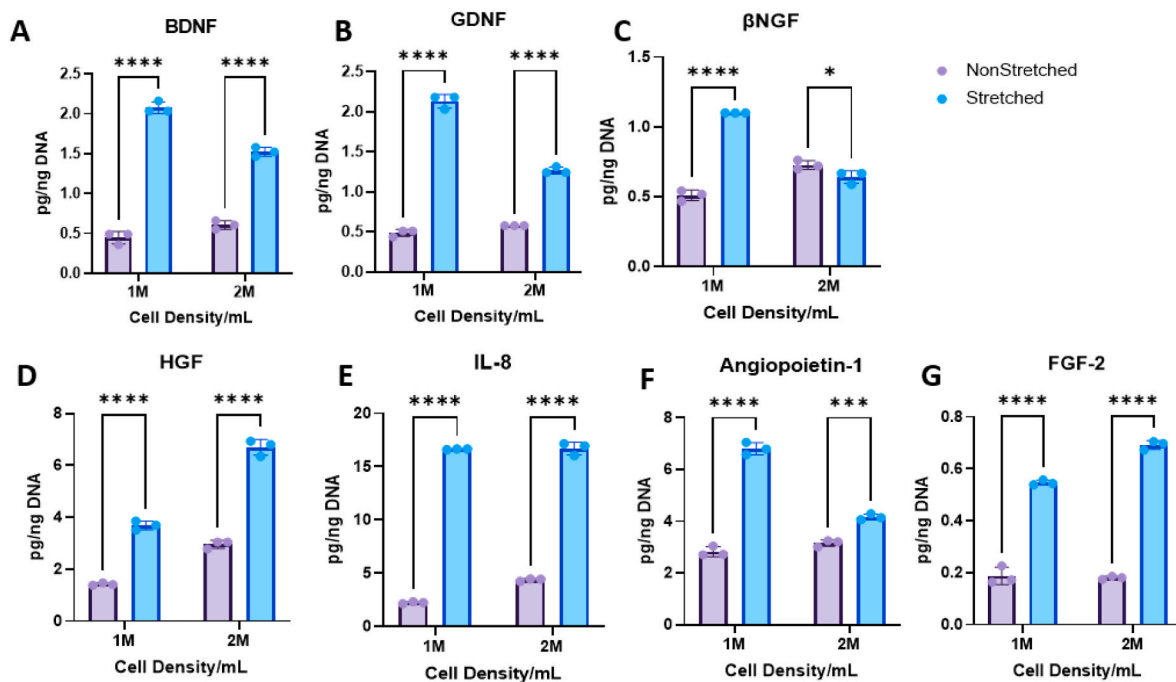
Fig. 5. Graphs depicting results from Luminex analysis normalized to DNA content performed on conditioned media from 3 mg/mL scaffolds over 24 h after 1 week of culture. Neurotrophins: **A.** Brain derived neurotrophic factor (BDNF) **B.** Glial derived neurotrophic factor (GDNF) **C.** Beta nerve growth factor (βNGF). Angiogenic factors: **D.** Hepatocyte growth factor (HGF) **E.** Interleukin 8 (IL-8) **F.** Angiopoietin-1 **G.** Fibroblast growth factor (FGF-2). Analysis performed with multiple t-tests. *p<0.05, ***p<0.001, ****p<0.0001 for n = 3/group.
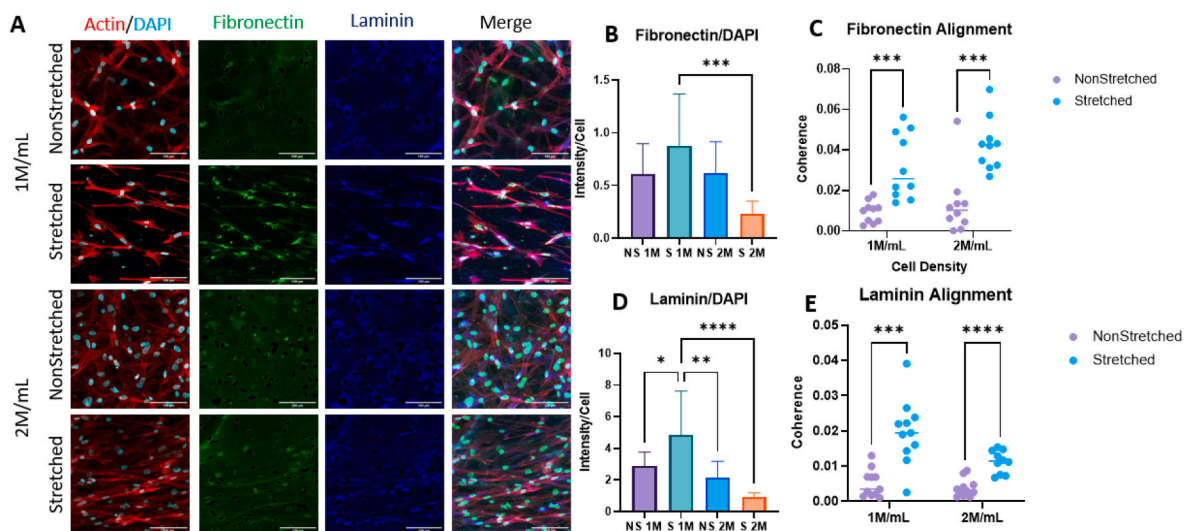

Fig. 6. A. Immunofluorescence images depicting f-actin (red), fibronectin (green), laminin (blue), and DAPI (cyan) in 3 mg/mL scaffolds after 1 week of culture. Scale bar = 100 μm. **B.** Intensity normalized to cell count of fibronectin. **C.** Coherence (alignment) of fibronectin in scaffolds. **D.** Intensity normalized to cell count of laminin. **E.** Coherence of laminin in scaffolds. Intensity analysis performed with one-way ANOVA with post-hoc Tukey's test. Orientation analysis performed with multiple t-tests. *p<0.05, **p<0.01, ***p<0.001, ****p<0.0001 for n = 12/group. (For interpretation of the references to color in this figure legend, the reader is referred to the Web version of this article.)

(Fig. 6). Fibronectin and laminin were chosen given their demonstrated roles in promoting nerve repair. Fibronectin plays a critical role in cell adhesion, migration, and proliferation, while laminin is a major component of the basement membrane and has been shown to play a crucial role in neural development and myelination [59–61]. In addition, both fibronectin and laminin are known to influence maturation and function of Schwann cells. Imaging and orientation analysis revealed a significant increase in alignment of both laminin and fibronectin in the stretched samples for both densities (Fig. 6c, e). Intensity analysis normalized to cell count showed the stretched 1 M/mL sample

had the greatest deposition of laminin compared to all other samples (Fig. 6d). The stretched 1 M/mL sample also showed the most deposition of fibronectin, while only significant against the stretched 2 M/mL group (Fig. 6b). Although not statistically significant against the NS 1 and 2 M/mL groups, the difference of means is considerable, and with a larger sample size the significance should improve enough that we are confident drawing conclusions from this analysis.

While many studies have investigated benefits of included fibronectin and laminin in peripheral nerve constructs with success, their deposition by ASCs in response to substrate alignment has not been

thoroughly explored [46,59–62]. Additionally, fibronectin expression increases during the early stages of Schwann cell differentiation and is required for the development of myelin-forming Schwann cells [63]. Furthermore, laminin expression is upregulated during Schwann cell differentiation and is required for the proper alignment and spacing of Schwann cells during myelin formation [60]. Laminin also plays a role in regulating the expression of myelin genes in Schwann cells, which are necessary for the formation and maintenance of myelin sheaths.

Interestingly, ASCs possess the ability to differentiate into "Schwann-like" cells and may be doing so in response to cell and fiber alignment within the grafts. Spontaneous Schwannogenic differentiation of MSCs cultured in aligned substrates has been documented [64], and while we have not stained against any Schwann cell markers in this study, ASC behavior suggests this as a possible explanation. Further investigation is needed to confirm this.

3.4. Potential mechanism (YAP)

To elucidate the mechanism driving ASCs' increased ECM deposition and elevated expression of both neurotrophic and angiogenic secretome in stretched gels, we stained against Yes-associated Protein (YAP). The YAP and TAZ (Transcriptional co-activator with PDZ-binding motif) pathway is a signaling pathway involved in regulating cell growth, proliferation, and differentiation. We hypothesized that the YAP/TAZ pathway activation was responsible for the elevated secretome in the stretched samples, as this pathway has been indicated in similar studies evaluating cell secretome response to stiffness and mechanical stimuli [48,49,65]. YAP and TAZ are transcriptional co-activators that are downstream effectors of the Hippo pathway, which is a signaling pathway involved in tissue homeostasis. In the absence of YAP/TAZ activation, they are phosphorylated by the Hippo pathway kinases and sequestered in the cytoplasm, leading to their degradation. Mechanical cues, such as substrate stiffness or fiber alignment, can activate the YAP/TAZ pathway and regulate its downstream effects. Specifically, when cells are subjected to mechanical forces that stretch or deform them, the resulting changes in cytoskeletal tension can lead to the activation and nuclear translocation of YAP/TAZ.

The YAP/TAZ pathway has been implicated in elevated angiogenic secretome of MSCs and ASCs through mechanotransduction of both substrate stiffness and fiber alignment [48,49]. After staining against YAP, we saw a significant increase in YAP intensity in the stretched samples (Fig. 7a–b). When we calculated the nuclear to cytoplasmic intensity ratio, however, we found that the non-stretched samples had a higher ratio with more proportional nuclear staining than the stretched group, which is usually found elevated when the pathway is triggered (Fig. 7c). Nuclear staining was evident in both non-stretched and stretched samples.

3.5. Mechanical testing

The stiffness of a hydrogel graft can not only influence embedded cell behavior, but native tissue behavior as well. Spontaneously self-assembled collagen fibrils tend to show poor mechanical strength under physiological conditions. These poor mechanical properties require crosslinking approaches to enhance the mechanical properties of collagen gels [66]. However, our gels do not utilize additional crosslinking techniques to improve mechanical properties. The native self-assembled collagen gels show mechanical properties proven to support neural cell growth. The self-assembled gels should show one of the following mechanical characteristics to support neuro-regenerative behavior. Low substrate stiffnesses (100–500 Pa) greatly favors neurons [66]. Higher substrate stiffnesses (1–10 kPa) influence cell differentiation and increase Schwann cell motility and proliferation [66,67]. Highest stiffnesses (>10 kPa) have been shown to be beneficial for axon guidance in peripheral nerve repair grafts.

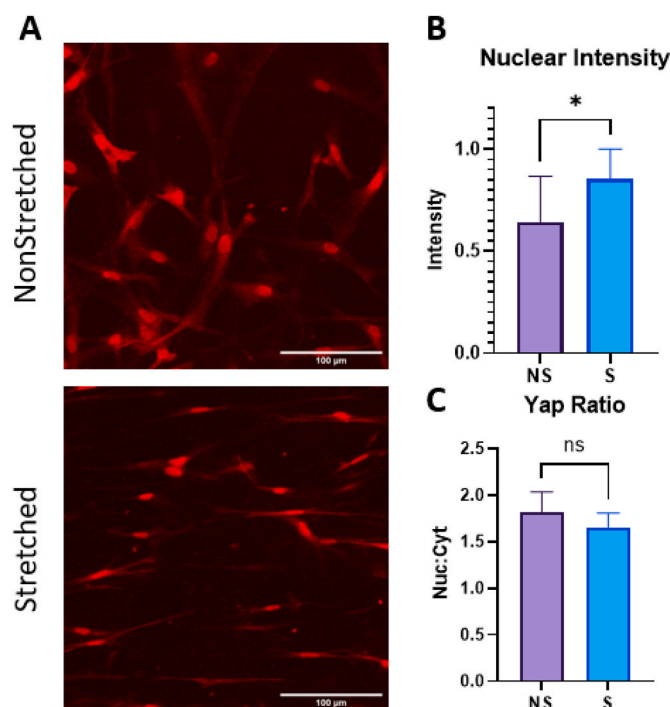Testing revealed Young's moduli of all samples within the 1–10 kPa

Fig. 7. A. Images visualizing YAP (red) in 3 mg/mL 1 M/mL scaffolds after 1 week of culture. Scale bar = 100 μm. **B.** Nuclear intensity of YAP staining in scaffolds. **C.** Nuclear:cytoplasmic staining ratio for YAP. Analysis performed with t-tests. *p<0.05 for n = 12/group. (For interpretation of the references to color in this figure legend, the reader is referred to the Web version of this article.)

range, previously proven ideal for Schwann cell migration [67] (Fig. 8c). Further, the S 1 M/mL sample had a Young's modulus of 6.5 ± 0.8 kPa, closest to a previously defined value of 7.45 kPa determined to be optimal for Schwann cell migration in a previously published study [68]. Results show stretched 3 mg/mL with 1 M/mL cellular density provides reported optimal mechanical properties to support Schwann cell migration.

3.6. Neurite outgrowth in vitro

To assess neurite outgrowth *in vitro*, partially dissociated, whole DRGs were seeded onto acellular and 1 M/mL non-stretched and stretched constructs (Fig. 9a). This partial dissociation method, along with full dissociation and whole DRG culture, has been well documented in other studies [45,67,69,70]. Several studies have included NGF or other growth factors in their neuronal media; because we wanted to investigate the effects of cell alignment and their increased cell secretome on neurite production and extension, this was omitted in our media. Orientation analysis of the outgrowing neurites revealed the highest concentration of neurite alignment in stretched samples around 0°, indicated by the peak (Fig. 9b). The same analysis of non-stretched samples revealed no peak or localization of fiber orientation, suggesting a random, unstructured organization of the neurites. The -10-degree peak in the stretched sample group suggests primarily horizontal orientation of outgrowing neurites, beneficial when trying to bridge a longer nerve gap. The smaller peak around 80° is perpendicular to the major orientation axis and represents the initial axon protrusion into the hydrogel. Often, axons growing into the hydrogel are unorganized close to the DRG, but as they grow farther from the source and into the aligned fiber network, they bend and eventually follow the orientation of cells and fibers.

Neurite counts were performed with a Scholl analysis tool, providing a count of neurons reaching a distance; in this case, measurements were
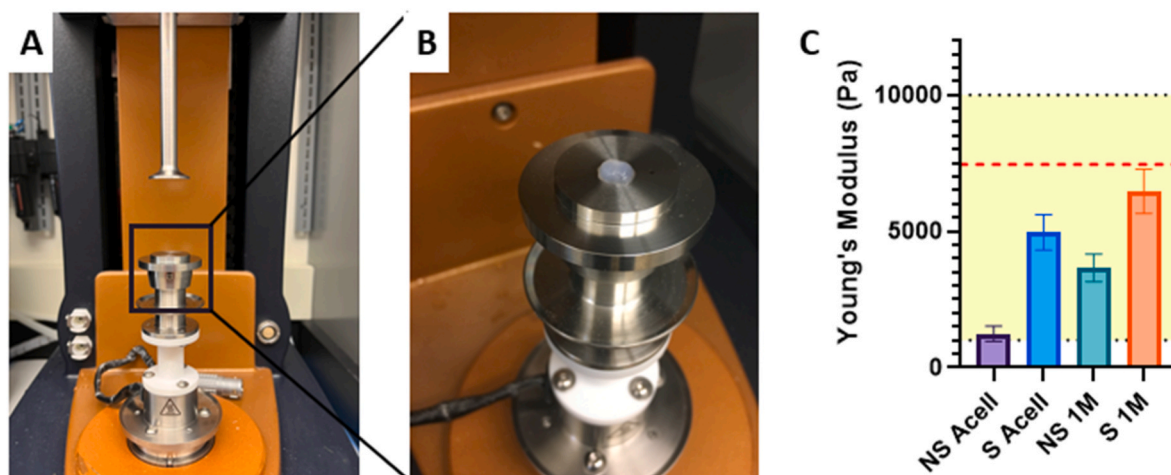
Fig. 8. A, B. Images of compression testing setup. **C.** Graph visualizing Young's modulus values for 3 mg/mL samples. Yellow shaded area representing 1–10 kPa and red dashed line representing 7.5 kPa target values. All groups significantly different at ****$p < 0.0001$ for n = 22–30/group. Analysis performed with one-way ANOVA and post-hoc Tukey's test. (For interpretation of the references to color in this figure legend, the reader is referred to the Web version of this article.)
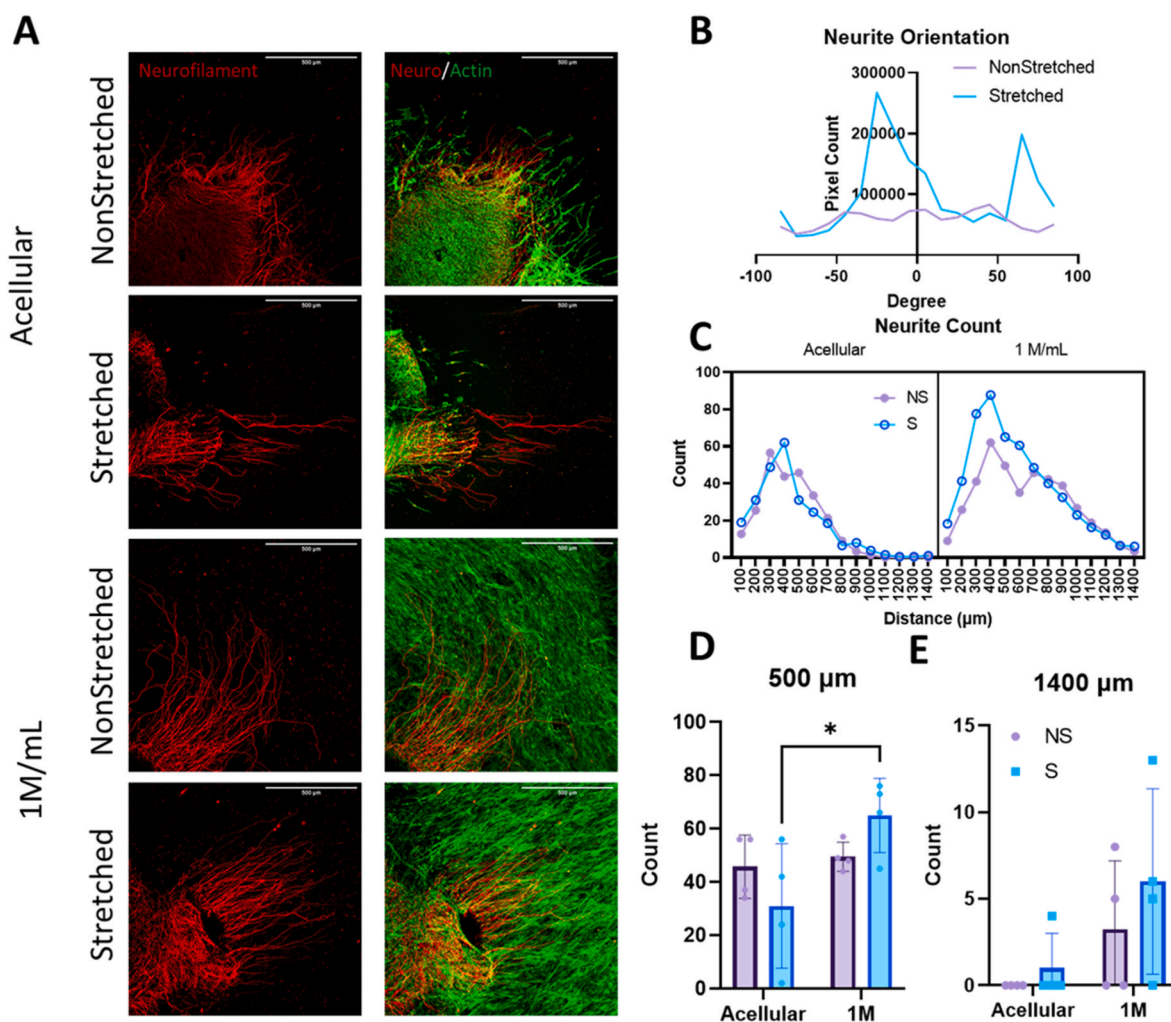

Fig. 9. A. Immunofluorescent images of neurite outgrowth after 48 h of co-culture on 3 mg/mL scaffolds visualizing neurofilament (red) and f-actin within cells (green). Scale bar = 500 μm **B.** Neurite orientation in 3 mg/mL 1 M/mL scaffolds, with values binned every 10°. **C, D, E.** Neurite count over a certain distance: (**C**) 100–1400 μm, (**D**) 500 μm, (**E**) 1400 μm. Analysis for **C** performed with three-way ANOVA. Analysis for **D** and **E** performed with two-way ANOVA and post-hoc Tukey's test. *$p < 0.05$ for n = 4/group. (For interpretation of the references to color in this figure legend, the reader is referred to the Web version of this article.)

taken every 100 μm from 0 to 1400 μm (Supplementary Figure 2). Sholl analyses function by creating concentric rings around a center point and measuring dendritic intersection with those rings. A count of neurites measured extending from the center of the DRG from 100 to 1400 μm shows the highest number of neurites reaching over both 500 and 1400 μm in the stretched 1 M/mL group (Fig. 9 d-e). Only the count at 500 μm for the S 1 M against the S acellular sample proved to be significantly different, however this is not surprising with the small sample size (n = 4/group). With increased sample size, we expect the significance to improve. Three-way ANOVA revealed significant sources of variation from both cell density and stretch (p<0.0001 and p = 0.0391 respectively) over all count distances, further supporting the argument for the stretched 1 M sample's advantage.

Although the cellular samples did have more neurite outgrowth (quantity and length) than the acellular samples, the differences were only significant when comparing the entire outgrowth profile with ANOVA and not at each outgrowth distance. While these data are promising, future studies should include a larger sample size and the neurite outgrowth evaluation at varying time points, as the cell presence may have greater influence on regeneration over longer periods of time. Further, the gold standard for DRG studies is harvesting from neonatal or newborn rats. This study was performed with DRGs from 3-week-old rats, which could contribute to limitations in neurite outgrowth, as DRGs become less proliferative as animals age. Additionally, the Sholl analysis is a radial assay, meaning all outgrowth from the center, not only in a certain direction is valued. If the distance was measured toward a specific endpoint along the axis of orientation (such as a nerve stump), we would expect to see further outgrowth in the stretched samples. Nerve stumps secrete additional neurotrophic factors such as NGF, GDNF and BDNF [71]. Through the encapsulation of ASCs into aligned collagen fiber gels, which deposited growth factors associated with the nerve stump, neuro-regenerative properties increased the outgrowth of neurites. Neurite outgrowth results are in alignment with other studies proving the advantage of anisotropic scaffold construction for peripheral nerve repair [45,70].

4. Conclusions and future directions

Here, we have demonstrated the fabrication and *in vitro* potential of our aligned collagen I scaffolds for use in peripheral nerve repair. Utilizing a silicone-based mold and pre-stretching with an in-house device, we showed significant and effective collagen fiber and cell alignment, increased neurotrophic and angiogenic secreted factors, and increased deposition and alignment of ECM components important for effective and directed nerve repair, possibly due to the mechanosensitive YAP/TAZ pathway. Furthermore, our *in vitro* model of DRG neurite outgrowth provided evidence supporting increased axonal regeneration and directional guidance governed by fiber and cell orientation within the scaffolds. Based on our results, an ideal scaffold would be one consisting of a stretched 3 mg/mL gel with a cellular density of 1 M/mL. The main novelty of our work comes from 1) the development of a custom uniaxial stretching device that allows co-alignment of ECM fibers and encapsulated cells, 2) a broad characterization of neuro-regenerative behavior of non-neural ASCs in aligned collagen fiber hydrogels for a long period of time in culture, and 3) its direct effect on neurite outgrowth.

This unique approach to the construction of the stretching device and accompanying molds allows for removal of the cell-laden, anisotropic hydrogel from the device after fabrication and its subsequent function as a nerve repair scaffold *in vivo*. The application of fiber alignment coupled with encapsulated cells can be used for customized nerve scaffolds, further promoting native-like tissues in nerve scaffolds for patient specificity and personalized to the anatomy of the nerve gap or injury. Notably, encapsulating pro-regenerative cells such as ASCs in 3D ECM hydrogels can provide a long-term living depot of neuro-regenerative molecules [72].

Some limitations of this study which can be investigated in the future are as follows. First, the *in vitro* nature of the current scaffold can be expanded to *in vivo* models to systematically assess neuro-regenerative potential of our scaffolds. To increase suturability, our hydrogels can be wrapped in mechanically compatible yet biocompatible materials such as small intestine submucosa wraps as previously demonstrated [10,11,73].

The current study looked at single time point for secretome analysis and neurite outgrowth. Future studies could explore additional time points to find optimal levels of neuro-regenerative growth factors. Assessing cell/fiber alignment and neurite length at varying time points would be beneficial to our understanding of longer-term behavior and effects of these scaffolds. Further investigation into potential mechanisms is also needed, including the YAP/TAZ pathway at varying substrate stiffness would help to confirm mechanism activation. As DRG neurite extension is also shown to be governed by YAP/TAZ [33], investigation on overlaid DRGs is also needed.

Finally, ASC behavior in our testbeds can be further evaluated. For instance, MSCs including ASCs have been shown to remodel ECM by matrix proteolysis to generate degradation microtracks that are utilized by pro-regenerative cells such as endothelial cells to form vascular network [42,74,75]. Further research into not only ECM remodeling by ASCs in aligned collagen fiber scaffolds but also its effects on neurite outgrowth would provide a more comprehensive understanding of the neuro-regenerative potential of our system.

Credit author statement

Mackenzie Lewis: Conceptualization, Methodology, Software, Validation, Formal analysis, Investigation, Writing – original draft, Writing – review & editing, Visualization. Gabriel David: Conceptualization, Methodology, Investigation, Writing – review & editing, Funding acquisition. Danielle Jacobs: Validation, Investigation, Writing – review & editing, Funding acquisition. Patrick Kuczwara: Investigation, Writing – review & editing. Moving his order up because of his significant contributions to the revision. Alan Woessner: Formal analysis, Visualization, Investigation, Writing – review & editing. Jin-Woo Kim: Resources, Writing – review & editing, Funding acquisition. Kyle Quinn: Resources, Writing – review & editing. Younghye Song: Conceptualization, Writing – original draft, Writing – review & editing, Supervision, Project administration, Funding acquisition.

Declaration of competing interest

The authors declare that they have no known competing financial interests or personal relationships that could have appeared to influence the work reported in this paper.

Data availability

Data will be made available on request.

Acknowledgements

Appendix A. Supplementary data

Supplementary data to this article can be found online at https://doi.

org/10.1016/j.mtbio.2023.100762.

References

[1] N.Y. Li, G.I. Onor, N.J. Lemme, J.A. Gil, Epidemiology of peripheral nerve injuries in sports, exercise, and recreation in the United States, 2009 - 2018, Phys. Sportsmed. 49 (2021) 355–362.

[2] M. Karsy, et al., Trends and cost analysis of upper extremity nerve injury using the national (nationwide) inpatient sample, World Neurosurg 123 (2019) e488–e500.

[3] B.S. Spearman, et al., Tissue-engineered peripheral nerve interfaces, Adv. Funct. Mater. 28 (2018) 1–18.

[4] C.R. Carvalho, J.M. Oliveira, R.L. Reis, Modern trends for peripheral nerve repair and regeneration: beyond the hollow nerve guidance conduit, Front. Bioeng. Biotechnol. 7 (2019) 1–30.

[5] M. Kasper, C. Deister, F. Beck, C.E. Schmidt, Bench-to-Bedside lessons learned: commercialization of an acellular nerve graft, Adv. Healthcare Mater. 9 (2020) 1–15.

[6] E. Verdú, et al., Alignment of collagen and laminin-containing gels improve nerve regeneration within silicone tubes, Restor. Neurol. Neurosci. 20 (2002) 169–179.

[7] P. Muangsanit, et al., Rapidly formed stable and aligned dense collagen gels seeded with Schwann cells support peripheral nerve regeneration, J. Neural. Eng. 17 (2020), 046036.

[8] S.H. Kim, et al., Anisotropically organized three-dimensional culture platform for reconstruction of a hippocampal neural network, Nat. Commun. 8 (2017), 14346.

[9] H. Seonwoo, et al., Hierarchically micro-and nanopatterned topographical cues for modulation of cellular structure and function, IEEE Trans. NanoBioscience 15 (2016) 835–842.

[10] C.S. Lacko, et al., Magnetic particle templating of hydrogels: engineering naturally derived hydrogel scaffolds with 3D aligned microarchitecture for nerve repair, J. Neural. Eng. 17 (2020), 016057.

[11] M. Kasper, et al., Development of a magnetically aligned regenerative tissue-engineered electronic nerve interface for peripheral nerve applications, Biomaterials 279 (2021), 121212.

[12] K. Belanger, et al., Recent strategies in tissue engineering for guided peripheral nerve regeneration, Macromol. Biosci. 16 (2016) 472–481.

[13] M. Antman-Passig, S. Levy, C. Gartenberg, H. Schori, O. Shefi, Mechanically oriented 3D collagen hydrogel for directing neurite growth, Tissue Eng. 23 (2017) 403–414.

[14] M.G. McCoy, et al., Collagen fiber orientation regulates 3D vascular network formation and alignment, ACS Biomater. Sci. Eng. 4 (2018) 2967–2976.

[15] C.C. Berry, J.C. Shelton, D.L. Bader, D.A. Lee, Influence of external uniaxial cyclic strain on oriented fibroblast-seeded collagen gels, Tissue Eng. 9 (2003) 613–624.

[16] Y.W. Chen, et al., Cyclic tensile stimulation enrichment of Schwann cell-laden auxetic hydrogel scaffolds towards peripheral nerve tissue engineering, Mater. Des. 195 (2020), 108982.

[17] J. Cao, et al., Induction of rat facial nerve regeneration by functional collagen scaffolds, Biomaterials 34 (2013) 1302–1310.

[18] Y. Cui, et al., Functional collagen conduits combined with human mesenchymal stem cells promote regeneration after sciatic nerve transection in dogs, J. Tissue Eng. Regen. Med. 12 (2018) 1285–1296.

[19] B. Marelli, C.E. Ghezzi, M. James-Bhasin, S.N. Nazhat, Fabrication of injectable, cellular, anisotropic collagen tissue equivalents with modular fibrillar densities, Biomaterials 37 (2015) 183–193.

[20] S. Yang, et al., Oriented collagen fiber membranes formed through counter-rotating extrusion and their application in tendon regeneration, Biomaterials 207 (2019) 61–75.

[21] V.T. Ribeiro-Resende, B. Koenig, S. Nichterwitz, S. Oberhoffner, B. Schlosshauer, Strategies for inducing the formation of bands of Büngner in peripheral nerve regeneration, Biomaterials 30 (2009) 5251–5259.

[22] N. Rbia, L.F. Bulstra, A.T. Bishop, A.J. van Wijnen, A.Y. Shin, A simple dynamic strategy to deliver stem cells to decellularized nerve allografts, Plast. Reconstr. Surg. 142 (2018) 402–413.

[23] F. Mathot, et al., Introducing human adipose-derived mesenchymal stem cells to Avance® nerve grafts and NeuraGen® nerve guides, J. Plast. Reconstr. Aesthetic Surg. 73 (2020) 1473–1481.

[24] J. Hu, Q.T. Zhu, X.L. Liu, Y. bin Xu, J.K. Zhu, Repair of extended peripheral nerve lesions in rhesus monkeys using acellular allogenic nerve grafts implanted with autologous mesenchymal stem cells, Exp. Neurol. 204 (2007) 658–666.

[25] L. Fan, Z. Yu, J. Li, X. Dang, K. Wang, Schwann-like cells seeded in acellular nerve grafts improve nerve regeneration, BMC Muscoskel. Disord. 15 (2014) 1–11.

[26] Y. Zhang, et al., A nerve graft constructed with xenogeneic acellular nerve matrix and autologous adipose-derived mesenchymal stem cells, Biomaterials 31 (2010) 5312–5324.

[27] X.H. Sun, et al., Improving nerve regeneration of acellular nerve allografts seeded with SCs bridging the sciatic nerve defects of rat, Cell. Mol. Neurobiol. 29 (2009) 347–353.

[28] L.N. Zhou, et al., A comparison of the use of adipose- derived and bone marrow-derived stem cells for peripheral nerve regeneration in vitro and in vivo, Stem Cell Res. Ther. 11 (2020) 1–16.

[29] Y. Wang, Y. Guo, D. Wang, J. Liu, J. Pan, Adipose stem cell-based clinical strategy for neural regeneration: a review of current opinion, Stem Cell. Int. 2019 (2019) 1–10.

[30] F.J. Vizoso, N. Eiro, S. Cid, J. Schneider, R. Perez-Fernandez, Mesenchymal stem cell secretome: toward cell-free therapeutic strategies in regenerative medicine, Int. J. Mol. Sci. 18 (2017) 1852.

[31] T. Xu, X. Zhang, X. Dai, Properties of electrospun aligned poly(lactic acid)/collagen fibers with nanoporous surface for peripheral nerve tissue engineering, Macromol. Mater. Eng. 307 (2022) 1–11.

[32] J. Xue, et al., Promoting cell migration and neurite extension along uniaxially aligned nanofibers with biomacromolecular particles in a density gradient, Adv. Funct. Mater. 30 (2020) 2002031.

[33] J. Ma, et al., Collagen modified anisotropic PLA scaffold as a base for peripheral nerve regeneration, Macromol. Biosci. 22 (2022) 1–10.

[34] L. Zhu, et al., Aligned PCL fiber conduits immobilized with nerve growth factor gradients enhance and direct sciatic nerve regeneration, Adv. Funct. Mater. 30 (2020) 2002610.

[35] F. Rao, et al., Aligned chitosan nanofiber hydrogel grafted with peptides mimicking bioactive brain-derived neurotrophic factor and vascular endothelial growth factor repair long-distance sciatic nerve defects in rats, Theranostics 10 (2020) 1590–1603.

[36] J. Du, et al., Prompt peripheral nerve regeneration induced by a hierarchically aligned fibrin nanofiber hydrogel, Acta Biomater. 55 (2017) 296–309.

[37] P. Muangsanit, V. Roberton, E. Costa, J.B. Phillips, Engineered aligned endothelial cell structures in tethered collagen hydrogels promote peripheral nerve regeneration, Acta Biomater. 126 (2021) 224–237.

[38] X. Dong, et al., Aligned microfiber-induced macrophage polarization to guide schwann-cell-enabled peripheral nerve regeneration, Biomaterials 272 (2021), 120767.

[39] M. Ghollasi, D. Poormoghadam, Enhanced neural differentiation of human-induced pluripotent stem cells on aligned laminin-functionalized polyethersulfone nanofibers; a comparison between aligned and random fibers on neurogenesis, J. Biomed. Mater. Res., Part A 110 (2022) 672–683.

[40] Y. Chai, et al., Structural alignment guides oriented migration and differentiation of endogenous neural stem cells for neurogenesis in brain injury treatment, Biomaterials 280 (2022), 121310.

[41] N. Rajan, J. Habermehl, M.F. Coté, C.J. Doillon, D. Mantovani, Preparation of ready-to-use, storable and reconstituted type I collagen from rat tail tendon for tissue engineering applications, Nat. Protoc. 1 (2007) 2753–2758.

[42] Y.H. Song, S.H. Shon, M. Shan, A.D. Stroock, C. Fischbach, Adipose-derived stem cells increase angiogenesis through matrix metalloproteinase-dependent collagen remodeling, Integr. Biol. 8 (2016) 205–215.

[43] A.E. Woessner, J.D. McGee, J.D. Jones, K.P. Quinn, Characterizing differences in the collagen fiber organization of skin wounds using quantitative polarized light imaging, Wound Repair Regen. 27 (2019) 711–714.

[44] Z. Püspöki, M. Storath, D. Sage, M. Unser, Transforms and operators for directional bioimage analysis: a survey, Focus on Bio-Image Informatics (2016) 69–93.

[45] A.R. D'Amato, et al., Exploring the effects of electrospun fiber surface nanotopography on neurite outgrowth and branching in neuron cultures, PLoS One 14 (2019) 1–18.

[46] S.D. Subramony, et al., The guidance of stem cell differentiation by substrate alignment and mechanical stimulation, Biomaterials 34 (2013) 1942–1953.

[47] R. Li, et al., Growth factors-based therapeutic strategies and their underlying signaling mechanisms for peripheral nerve regeneration, Acta Pharmacol. Sin. 41 (2020) 1289–1300.

[48] S. Wan, et al., FAK- and YAP/TAZ dependent mechanotransduction pathways are required for enhanced immunomodulatory properties of adipose-derived mesenchymal stem cells induced by aligned fibrous scaffolds, Biomaterials 171 (2018) 107–117.

[49] P. Bandaru, et al., Mechanical cues regulating proangiogenic potential of human mesenchymal stem cells through YAP-mediated mechanosensing, Small 16 (2020) 1–13.

[50] N.Z. Alsmadi, et al., Glial-derived growth factor and pleiotrophin synergistically promote axonal regeneration in critical nerve injuries, Acta Biomater. 78 (2018) 165–177.

[51] M.-H. Chen, P.-R. Chen, M.-H. Chen, S.-T. Hsieh, F.-H. Lin, Gelatin–tricalcium phosphate membranes immobilized with NGF, BDNF, or IGF-1 for peripheral nerve repair: an in vitro and in vivo study, J. Biomed. Mater. Res., Part A 79 (2006) 846–857.

[52] Y. Lu, et al., Fibroblast growth factor 21 facilitates peripheral nerve regeneration through suppressing oxidative damage and autophagic cell death, J. Cell Mol. Med. 23 (2019) 497–511.

[53] F. Zhang, Y. Miao, Q. Liu, S. Li, J. He, Changes of pro-inflammatory and anti-inflammatory macrophages after peripheral nerve injury, RSC Adv. 10 (2020) 38767–38773.

[54] C. Chang, et al., Effects of mesenchymal stem cell-derived paracrine signals and their delivery strategies, Adv. Healthcare Mater. 10 (2021) 1–17.

[55] G.K. Tofaris, P.H. Patterson, K.R. Jessen, R. Mirsky, Denervated Schwann cells attract macrophages by secretion of leukemia inhibitory factor (LIF) and monocyte chemoattractant protein-1 in a process regulated by interleukin-6 and LIF, J. Neurosci. 22 (2002) 6696–6703.

[56] L. Qiu, et al., Cartilage oligomeric matrix protein angiopoeitin-1 provides benefits during nerve regeneration in vivo and in vitro, Ann. Biomed. Eng. 43 (2015) 2924–2940.

[57] K.R. Ko, J. Lee, D. Lee, B. Nho, S. Kim, Hepatocyte growth factor (HGF) promotes peripheral nerve regeneration by activating repair schwann cells, Sci. Rep. 8 (2018) 1–14.

[58] M. Boldyreva, et al., Plasmid-based gene therapy with hepatocyte growth factor stimulates peripheral nerve regeneration after traumatic injury, Biomed. Pharmacother. 101 (2018) 682–690.

[59] L. Parisi, et al., A glance on the role of fibronectin in controlling cell response at biomaterial interface, Jpn. Dent. Sci. Rev. 56 (2020) 50–55.

[60] Z.L. Chen, S. Strickland, Laminin γ1 is critical for Schwann cell differentiation, axon myelination, and regeneration in the peripheral nerve, J. Cell Biol. 163 (2003) 889–899.

[61] K.V. Panzer, et al., Tissue engineered bands of büngner for accelerated motor and sensory axonal outgrowth, Front. Bioeng. Biotechnol. 8 (2020) 1–19.

[62] W. Xue, et al., Regulation of schwann cell and DRG neurite behaviors within decellularized peripheral nerve matrix, ACS Appl. Mater. Interfaces 14 (2022) 8693–8704.

[63] E. Torres-Mejía, et al., Sox2 controls Schwann cell self-organization through fibronectin fibrillogenesis, Sci. Rep. 10 (2020) 1–17.

[64] X. Hu, et al., Electric conductivity on aligned nanofibers facilitates the transdifferentiation of mesenchymal stem cells into schwann cells and regeneration of injured peripheral nerve, Adv. Healthcare Mater. 9 (2020) 1901570.

[65] S.R. Caliari, S.L. Vega, M. Kwon, E.M. Soulas, J.A. Burdick, Dimensionality and spreading influence MSC YAP/TAZ signaling in hydrogel environments, Biomaterials 103 (2016) 314–323.

[66] W.-H. Huang, et al., Collagen for neural tissue engineering: materials, strategies, and challenges, Mater. Today Bio 20 (2023), 100639.

[67] G. Rosso, I. Liashkovich, P. Young, D. Röhr, V. Shahin, Schwann cells and neurite outgrowth from embryonic dorsal root ganglions are highly mechanosensitive, Nanomed. Nanotechnol. Biol. Med. 13 (2017) 493–501.

[68] Y. Gu, et al., The influence of substrate stiffness on the behavior and functions of Schwann cells in culture, Biomaterials 33 (2012) 6672–6681.

[69] A. Bozkurt, et al., In vitro assessment of axonal growth using dorsal root ganglia explants in a novel three-dimensional collagen matrix, Tissue Eng. 13 (2007) 2971–2979.

[70] W. Martens, et al., Human dental pulp stem cells can differentiate into Schwann cells and promote and guide neurite outgrowth in an aligned tissue-engineered collagen construct in vitro, Faseb. J. 28 (2014) 1634–1643.

[71] J.G. Boyd, T. Gordon, Neurotrophic factors and their receptors in axonal regeneration and functional recovery after peripheral nerve injury, Mol. Neurobiol. 27 (2003) 277–323.

[72] M.E. Wechsler, V.V. Rao, A.N. Borelli, K.S. Anseth, Engineering the MSC secretome : a hydrogel focused approach, Adv. Healthcare Mater. 10 (2021), 2001948.

[73] G. Cao, et al., Small intestinal submucosa: superiority, limitations and solutions, and its potential to address bottlenecks in tissue repair, J. Mater. Chem. B 7 (2019) 5038–5055.

[74] C.M. Ghajar, et al., Mesenchymal cells stimulate capillary morphogenesis via distinct proteolytic mechanisms, Exp. Cell Res. 316 (2010) 813–825.

[75] K.M. Schultz, K.A. Kyburz, K.S. Anseth, Measuring dynamic cell-material interactions and remodeling during 3D human mesenchymal stem cell migration in hydrogels, Proc. Natl. Acad. Sci. U.S.A. 112 (2015) E3757–E3764.